

PHYSICAL DUST MODELS FOR THE EXTINCTION TOWARD SUPERNOVA 2014J IN M82

JIAN GAO^{1,2}, B. W. JIANG¹, AIGEN LI², JUN LI¹, AND XIAOFENG WANG³*Draft version 2015.7.3.24*

ABSTRACT

Type Ia supernovae (SNe Ia) are powerful cosmological “standardizable candles” and the most precise distance indicators. However, a limiting factor in their use for precision cosmology rests on our ability to correct for the dust extinction toward them. SN 2014J in the starburst galaxy M82, the closest detected SN Ia in three decades, provides unparalleled opportunities to study the dust extinction toward an SN Ia. In order to derive the extinction as a function of wavelength, we model the color excesses toward SN 2014J, which are observationally derived over a wide wavelength range in terms of dust models consisting of a mixture of silicate and graphite. The resulting extinction laws steeply rise toward the far ultraviolet, even steeper than that of the Small Magellanic Cloud (SMC). We infer a visual extinction of $A_V \approx 1.9$ mag, a reddening of $E(B - V) \approx 1.1$ mag, and a total-to-selective extinction ratio of $R_V \approx 1.7$, consistent with that previously derived from photometric, spectroscopic, and polarimetric observations. The size distributions of the dust in the interstellar medium toward SN 2014J are skewed toward substantially smaller grains than that of the Milky Way and the SMC.

Subject headings: dust, extinction — galaxies: ISM — galaxies: individual (Messier 82) — supernovae: individual (SN 2014J)

1. INTRODUCTION

Type Ia supernovae (SNe Ia) are considered to be one of the most precise tools for determining astronomical distances (Howell 2011). Because of their high luminosity and relatively small dispersion at the maxima of their bolometric light curves, they are commonly utilized as cosmological “standardizable candles”. The accelerated expansion of the Universe and the presence of dark energy were discovered through SNe Ia used as standardizable candles (Riess et al. 1998; Perlmutter et al. 1999). The effectiveness of SNe Ia as distance indicators and standard candles is hampered by the systematic uncertainties related to their explosion mechanism and progenitor systems, and more importantly, the line-of-sight extinction. The distance d measured in parsec to a SN is $\lg d = 0.2(m_\lambda - M_\lambda + 5 - A_\lambda)$, where m_λ and M_λ are its apparent and absolute magnitudes at wavelength λ , and A_λ is the extinction. As it is not easy to directly measure A_λ , one often measures the color excess (or reddening) $E(\lambda - V) \equiv A_\lambda - A_V$, where A_V is the extinction in the V-band (centered around 5500 Å). SN reddening is often measured by comparing the observed SN colors to a zero-reddening locus.

Cardelli et al. (1989; CCM) found that the Galactic extinction curves (or extinction laws) — the wave-

length dependencies of the extinction — can be closely parametrized by the total-to-selective extinction ratio $R_V \equiv A_V/E(B - V)$, where the B-band centers around 4400 Å (also see Fitzpatrick 1999, hereafter FTZ). Astronomers often derive R_V for SNe Ia by fitting the observed $E(\lambda - V)$ with the R_V -based CCM formula. Once R_V is determined, one can apply the CCM-formula (or some other parameterizations) to derive A_λ . However, we caution that the CCM- and FTZ-parameterizations have been derived for Galactic sightlines with $2 < R_V < 5$, and may not be valid for external galaxies. Note that the CCM formula is not even applicable to the Large and Small Magellanic Clouds (LMC, SMC; Gordon et al. 2003).

SNe Ia are so rare that nearby SNe Ia ($d < 5$ Mpc) are detected only about once a decade. SN 2014J, discovered in the nearby starburst galaxy M82 at a distance of $d \approx 3.5$ Mpc (Dalcanton et al. 2009), is the nearest SN Ia seen in the last three decades. Its proximity offers an unprecedented opportunity to study the extinction and reddening toward a SN Ia. The aim of this Letter is to derive R_V and A_λ by fitting the reddening curve obtained by Amanullah et al. (2014) during the epoch range of $[-5, +5]$ days around its peak brightness (§2) using the silicate-graphite model (§3). The results are presented in §3, discussed in §4, and summarized in §5.

2. COLOR-EXCESS CURVES OF SN 2014J

Various studies have been carried out to determine the R_V value for the sightline toward SN 2014J (e.g., see Amanullah et al. 2014; Foley et al. 2014; Goobar et al. 2014; Marion et al. 2015; Welty et al. 2014). More specifically, based on the UV to near-IR photometry of

¹ Department of Astronomy, Beijing Normal University, Beijing 100875, China; jiangao@bnu.edu.cn, bjiang@bnu.edu.cn

² Department of Physics and Astronomy, University of Missouri, Columbia, MO 65211, USA; lia@missouri.edu

³ Department of Physics, and Center for Astrophysics, Tsinghua University, Beijing 100084, China wang_xf@mail.tsinghua.edu.cn

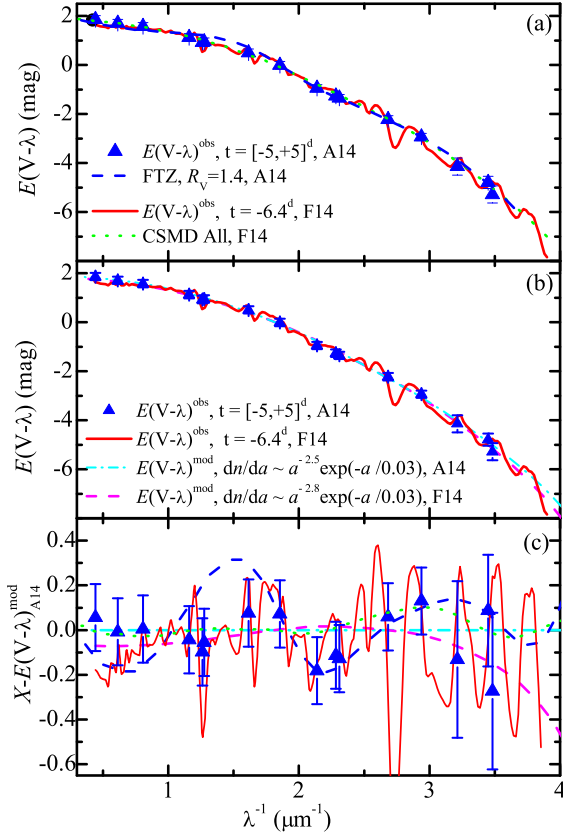


FIG. 1.— (a) Comparison of the color-excess curve of F14 (red solid line) with that of A14 (blue triangles). The blue dashed line is the best-fit FTZ model of A14, while the green dotted line is the best-fit two-component model (i.e., a combination of interstellar reddening and circumstellar scattering) for all epochs (“CSMD All”) of SN 2014J of F14. (b) Comparison of the color-excess curves of F14 (red solid line) and A14 (blue triangles) with our model predictions (magenta dashed line for F14, and cyan dot-dashed line for A14). (c) Residuals between our model color-excess $E(V - \lambda)_{\text{A14}}^{\text{mod}}$ for A14 and (i) the data points of A14 (blue triangles), (ii) the FTZ fit of A14 (blue dashed line), (iii) the color-excess curve of F14 (red solid line), (iv) the CSMD fit of F14 (green dotted line), and (v) our model color-excess for F14 (magenta dashed line).

SN 2014J obtained with the WFC3 filters aboard the *Hubble Space Telescope* (HST) and ground-based telescopes, Amanullah et al. (2014, hereafter A14) determined the reddening curve $E(\lambda - V)$ for SN 2014J over a wide wavelength range by comparing the colors of SN 2014J with that of SN 2011fe, a reddening-free SN Ia. They derived $R_V \approx 1.4 \pm 0.1$ by fitting the observationally determined $E(\lambda - V)$ with three template extinction laws: an MW-type law as parameterized by CCM or FTZ (see Figure 1a), a third-order polynomial SALT2 law (see Betoule et al. 2014), and a power-law parameterization $A_\lambda \sim \lambda^p$ which was shown to be a good approximation for multiple scattering scenarios (Goobar 2008).

We note that A14 shifted the effective wavelengths of the HST/WFC3 filters (see their Figure 3). In the following, we adopt the wavelength-shifted color-excess data of

A14.

Foley et al. (2014, hereafter F14) determined the extinction curve toward SN 2014J at $t = -6.4, +24.1$ d by comparing the UV/near-IR SED of SN 2014J with that of SN 2011fe. As shown in Figure 1, the color-excess curve of F14 closely resembles that of A14. The difference between the F14 curve and that of A14, on average, is ~ 0.19 mag (see Figure 1c). Using FTZ and CCM models, F14 derived $R_V \approx 1.66 \pm 0.03$ and $\approx 1.44 \pm 0.03$ for SN 2014J, respectively. F14 also argued that a two-component model (CSMD) with both a circumstellar scattering component of $A_\lambda \sim \lambda^{-2.57}$ and an FTZ interstellar reddening component of $R_V \approx 2.6$ could best account for the observed properties of SN 2014J.

3. DUST MODEL

We consider the silicate-graphite grain model that consists of amorphous silicate and graphite (Draine & Lee 1984). We adopt the same exponentially cutoff power-law size distribution for both components: $dn_i/da = n_H B_i a^{-\alpha} \exp(-a/a_b)$ for the size range of $50 \text{ \AA} < a < 1 \text{ \mu m}$, where a is the spherical radius of the dust, n_H is the number density of H nuclei, dn_i is the number density of dust of type i with radii in the interval $[a, a + da]$, α and a_b are, respectively, the power index and exponential cutoff size, and B_i is a constant related to the total amount of dust of type i . The total extinction at wavelength λ is given by

$$A_\lambda/N_H = (2.5 \log e) \sum_i \int da \frac{1}{n_H} \frac{dn_i}{da} C_{\text{ext},i}(a, \lambda), \quad (1)$$

where the summation is over the two grain types, N_H (n_H) is the H column (number) density, and $C_{\text{ext},i}(a, \lambda)$ is the extinction cross section of grain type i of size a at wavelength λ calculated from Mie theory using the optical constants of Draine & Lee (1984).

For a given set of parameters α and a_b , we derive the constant B_i from the abundances of the dust-forming elements. Let $[X/H]_{\text{ISM}}$ be the total interstellar abundance of element X (i.e., Fe, Mg, Si, O, and C) relative to H in the interstellar medium (ISM) of M82, $[X/H]_{\text{gas}}$ be the amount of X in the gas phase, $[X/H]_{\text{dust}}$ be the amount of X contained in dust (obviously, $[X/H]_{\text{dust}} = [X/H]_{\text{ISM}} - [X/H]_{\text{gas}}$), and μ_X be the atomic weight of X. Let $\rho_{\text{sil}} \approx 3.5 \text{ g cm}^{-3}$ and $\rho_{\text{gra}} \approx 2.24 \text{ g cm}^{-3}$, respectively, be the mass density of amorphous silicate and graphite. For a chosen set of dust depletions, we derive B_i from the dust size distributions:

$$n_H B_{\text{sil}} = \frac{\mu_{\text{Fe}} [\text{Fe}/H]_{\text{dust}} + \mu_{\text{Mg}} [\text{Mg}/H]_{\text{dust}} + \mu_{\text{Si}} [\text{Si}/H]_{\text{dust}}}{\int da (4\pi/3) a^3 \rho_{\text{sil}} a^{-\alpha} \exp(-a/a_b)} \quad (2)$$

$$n_H B_{\text{gra}} = \frac{\mu_{\text{C}} [\text{C}/H]_{\text{dust}}}{\int da (4\pi/3) a^3 \rho_{\text{gra}} a^{-\alpha} \exp(-a/a_b)}, \quad (3)$$

where we assume a stoichiometric composition of

$\text{Mg}_{2x}\text{Fe}_{2(1-x)}\text{SiO}_4$ for amorphous silicate.

M82 is a prototypical starburst galaxy, experiencing a major star formation episode in its nuclear region, with strong superwind and SN activity. Origlia et al. (2004) obtained the stellar abundances in the nuclear region of M82, and compared them with those of the hot gas derived from the nuclear X-ray spectra. Compared with the solar abundance of Grevesse & Sauval (1998), both the cool stars and the hot gas in M82 suggest a reduction of Fe/H by $\approx -0.35 \pm 0.2$ dex (i.e., $[\text{Fe}/\text{H}]_{\text{ISM}} \approx 14.1$ ppm) and an overall Si/Fe and Mg/Fe enhancement by ~ 0.4 and 0.5 dex, respectively (i.e., $[\text{Si}/\text{H}]_{\text{ISM}} \approx 35.5$ ppm, $[\text{Mg}/\text{H}]_{\text{ISM}} \approx 44.7$ ppm). Oxygen is enhanced by ~ 0.3 dex in stars and reduced by ~ 0.2 dex in the hot gas.⁴ The stellar abundance of C derived by Origlia et al. (2004) is only $\sim 1/4$ of solar (i.e., $[\text{C}/\text{H}]_{\text{ISM}} \approx 83.2$ ppm).

Similar to the Galactic ISM, we assume in M82 that Fe, Mg and Si are all locked up in silicate dust (i.e., $[\text{Fe}/\text{H}]_{\text{dust}} \approx [\text{Fe}/\text{H}]_{\text{ISM}} \approx 14.1$ ppm, $[\text{Mg}/\text{H}]_{\text{dust}} \approx [\text{Mg}/\text{H}]_{\text{ISM}} \approx 44.7$ ppm, $[\text{Si}/\text{H}]_{\text{dust}} \approx [\text{Si}/\text{H}]_{\text{ISM}} \approx 35.5$ ppm; Origlia et al. 2004). For carbon, it is less clear. In the Galactic ISM, a substantial fraction ($\approx 42\%$)⁵ of the total carbon abundance is in the gas phase ($[\text{C}/\text{H}]_{\text{gas}} \approx 140$ ppm, Cardelli et al. 1996). For carbon dust (i.e., graphite) in M82, we will consider three cases $[\text{C}/\text{H}]_{\text{dust}} = [\text{C}/\text{H}]_{\text{ISM}} \approx 83.2$ ppm (i.e., all C is locked up in dust), $[\text{C}/\text{H}]_{\text{dust}} = 1/2 [\text{C}/\text{H}]_{\text{ISM}} \approx 41.6$ ppm, and $[\text{C}/\text{H}]_{\text{dust}} = 0$ ppm (i.e., all C is in the gas phase and the dust model only consists of amorphous silicate). With $[\text{C}/\text{H}]_{\text{dust}} = 41.6$ ppm, the model has a silicate-to-graphite mass ratio of $m_{\text{sil}}/m_{\text{gra}} \approx 10$. This is close to that of the SMC ($m_{\text{sil}}/m_{\text{gra}} \approx 12$, Li et al. 2006).

To facilitate a direct comparison with the color excesses $E(V - \lambda)^{\text{obs}}$ derived by A14 for SN 2014J, we first calculate A_λ from Eq.1 and then convert to reddening $E(V - \lambda)^{\text{mod}} \equiv A_V - A_\lambda$. For simplicity, the model color-excess has not been convolved with the HST/WFC3 filters. We evaluate the goodness of fitting by

$$\chi^2_{\text{d.o.f}} = \frac{\sum_{j=1}^{N_{\text{obs}}} [E(V - \lambda_j)^{\text{mod}} - E(V - \lambda_j)^{\text{obs}}]^2 / \sigma(\lambda_j)^2}{N_{\text{obs}} - N_{\text{para}}}, \quad (4)$$

where $E(V - \lambda_j)^{\text{obs}}$ is the observed color excess toward SN 2014J at wavelength λ_j derived by A14, $\sigma(\lambda_j)$ is the uncertainty of $E(V - \lambda_j)^{\text{obs}}$, $E(V - \lambda_j)^{\text{mod}}$ is the model color excess at λ_j , $N_{\text{obs}} = 16$ is the number of observational data points, and N_{para} is the number of adjustable parameters.

4. RESULTS

⁴ An accurate knowledge of the O/H abundance is not required. The amount of O/H locked up in dust is controlled by Si/H: $[\text{O}/\text{H}]_{\text{dust}} = 4 [\text{Si}/\text{H}]_{\text{dust}}$ for a silicate composition of $\text{Mg}_{2x}\text{Fe}_{2(1-x)}\text{SiO}_4$.

⁵ We take the Galactic interstellar carbon abundance to be solar: $[\text{C}/\text{H}]_{\text{ISM}} \approx [\text{C}/\text{H}]_{\odot} \approx 331$ ppm (Grevesse & Sauval 1998).

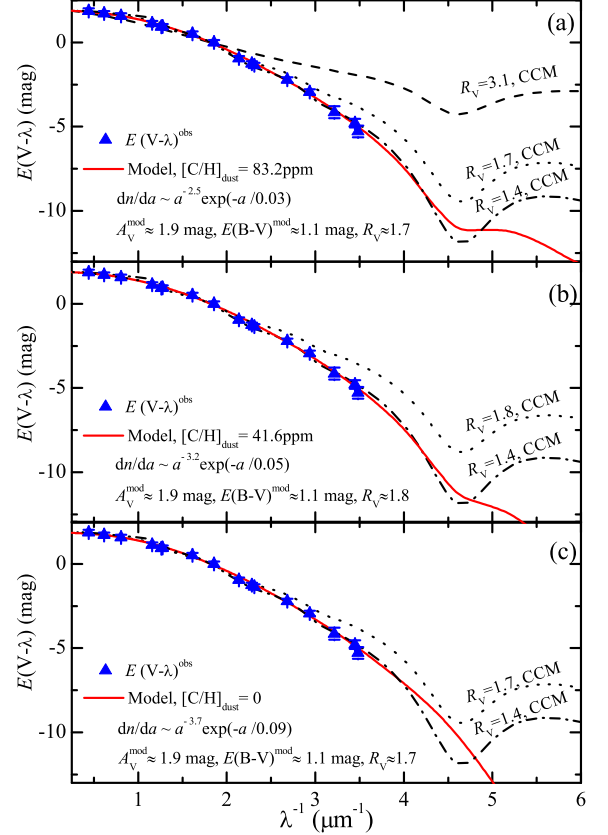


FIG. 2.— Fitting the color excesses between -5 and $+5$ days from the B maximum of SN 2014J (blue triangles; A14) with the silicate-graphite model (red solid lines), assuming all (a), half (b), and none (c) of the carbon elements are depleted in graphite. The dotted lines plot the CCM reddening curves with the R_V values corresponding to that of the models (a: $R_V = 1.7$, b: $R_V = 1.8$, c: $R_V = 1.7$). For comparison, the Galactic average of $R_V = 3.1$ (dashed line) and CCM reddening curve of $R_V = 1.4$ (dot-dashed line) are also shown.

In fitting the color excesses of SN 2014J observationally determined by A14, we have three parameters (i.e., $N_{\text{para}} = 3$): α , a_b , and N_{H} . As shown in Figure 2, excellent fits to the observed color excesses can be achieved by varying α and a_b for a given $[\text{C}/\text{H}]_{\text{dust}}$ (see Table 1).

The best-fit models derive $A_V \approx 1.9$ mag, $E(B - V) \approx 1.1$ mag, and $R_V \approx 1.7$. The reddening and A_V are consistent with those reported earlier, i.e., $E(B - V) \approx 0.8 - 1.3$ mag and $A_V \sim 1.8 - 2.0$ mag (Amanullah et al. 2014; Ashall et al. 2014; Foley et al. 2014; Goobar et al. 2014; Welty et al. 2014), while the model R_V values are somewhat larger than most of the earlier results, i.e., $R_V \sim 1.4$ (Amanullah et al. 2014; Brown et al. 2015; Goobar et al. 2014; Marion et al. 2015).

The best-fit models suggest $N_{\text{H}} \approx 1.3 - 3.3 \times 10^{22} \text{ cm}^{-2}$ for the sightline toward SN 2014J, somewhat higher than that of the hot gas in M82, $N_{\text{H}} \approx (7.9 \pm 0.7) \times 10^{21} \text{ cm}^{-2}$, derived from *Chandra* observations (Origlia et al. 2004).

In Figure 3, we show the best-fit models shown in Figure 2 in terms of A_λ/A_V . For comparison, we also show the CCM reddening curve of $R_V = 1.4$, the average extinction curves for the MW ($R_V = 3.1$) and the SMC

TABLE 1
MODEL PARAMETERS AND RESULTS

$[\text{C}/\text{H}]_{\text{dust}}^{\text{a}}$ (ppm)	$n_{\text{H}} B_{\text{gra}}$ ($\text{cm}^{\alpha-1}/\text{H}$)	$n_{\text{H}} B_{\text{sil}}$ ($\text{cm}^{\alpha-1}/\text{H}$)	α	a_b (μm)	N_{H} (10^{22} cm^{-2})	$\chi^2/\text{d.o.f}$	$E(\text{B}-\text{V})$ (mag)	A_V (mag)	R_V
83.2	1.3×10^{-19}	4.0×10^{-20}	2.5	0.03	1.3	0.45	1.1	1.9	1.7
41.6	1.0×10^{-23}	1.6×10^{-24}	3.2	0.05	1.9	0.47	1.1	1.9	1.8
0	0	1.2×10^{-26}	3.7	0.09	3.3	0.53	1.1	1.9	1.7
83.2 ^b	3.7×10^{-23}	1.4×10^{-23}	3.1	0.05	1.6	0.51	1.1	2.0	1.8
41.6 ^b	2.5×10^{-24}	4.7×10^{-25}	3.3	0.06	2.1	0.51	1.1	1.9	1.8
83.2 ^c	4.7×10^{-19}	1.4×10^{-19}	2.4	0.03	1.3	0.43	1.1	1.9	1.7
83.2 ^d	3.0×10^{-21}	9.1×10^{-22}	2.8	0.03	1.5	2.96	1.1	1.9	1.7

^a Assumed carbon depletion in graphite or amorphous carbon.

^b Amorphous carbon.

^c The F218W and F225W data points of A14 were excluded.

^d Best fit for F14 at $t = -6.4 d$.

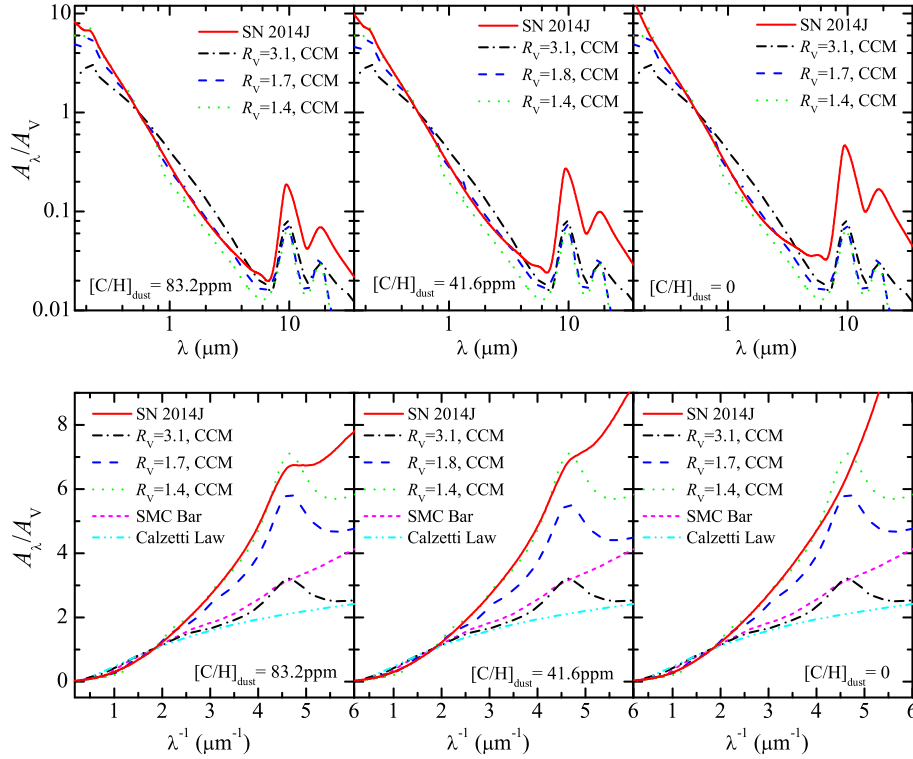


FIG. 3.— Comparison of the model extinction curves of SN 2014J (red solid) with that for the CCM $R_V = 3.1$ (black dash-dotted), $R_V = 1.4$ (green dotted), $R_V = 1.7$ or 1.8 (blue dashed), the SMC bar (magenta short dashed), and the Calzetti attenuation law for starbursts (cyan dash-dot-dotted).

bar. The model extinction laws for SN 2014J all exhibit a rapid far-UV rise which is even much steeper than that of the SMC bar. Unlike the SMC bar, the SN 2014J extinction laws display an appreciable extinction bump at 2175 \AA for $[\text{C}/\text{H}]_{\text{dust}} > 0$. We also show in Figure 3 the extinction curves predicted from the CCM formula with the corresponding model-derived R_V values (i.e., $R_V \approx 1.7, 1.8$). It is seen that they substantially differ from that calculated from the dust models.

As mentioned in §2, A14 shifted the effective wave-

lengths of the HST/WFC3 filters, especially for the bluest F218W and F225W bands, which are highly dependent on the SN spectrum and the reddening law. To examine the effects of the wavelength-shifts, we have also modeled the observed color-excess curve of A14 by excluding the F218W and F225W data points (which could be most affected). The results do not show any appreciable differences (see Table 1). We have also modeled the F14 curve (at $t = -6.4 d$). As shown in Figure 1b and Table 1, the model extinction curves and the result-

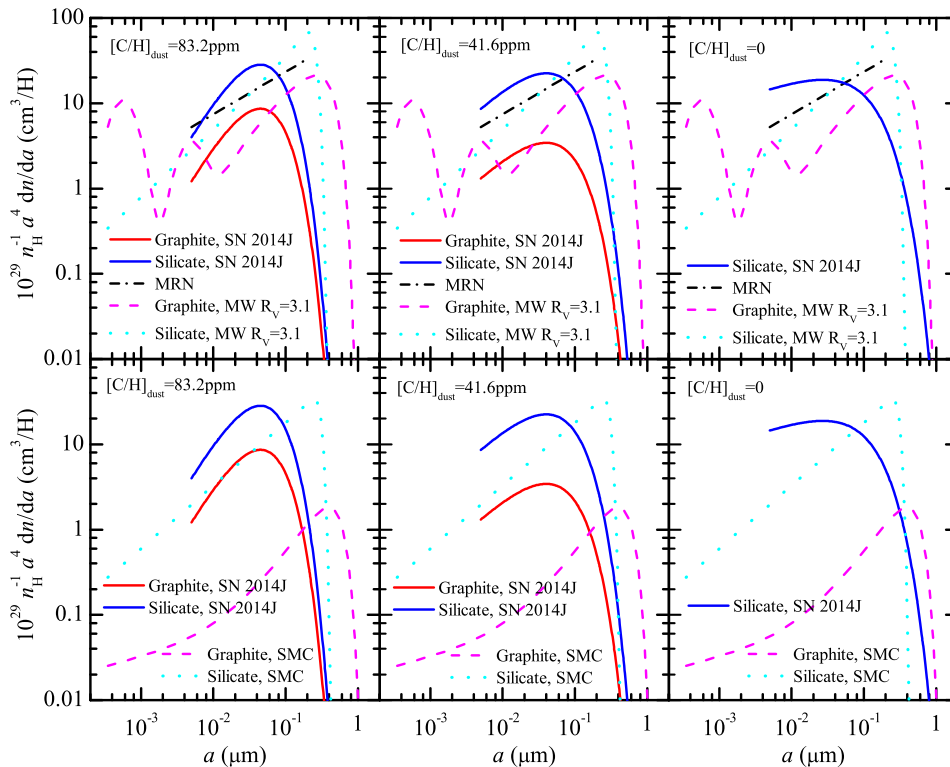


FIG. 4.— Comparison of the size distributions of silicate (blue solid) and graphite (red solid) derived for SN 2014J with that of the MW $R_V = 3.1$ and SMC (silicate: cyan dotted; graphite: magenta dashed; see WD01). Also shown is the MRN size distribution (black dot-dashed).

ing A_V and R_V are very close to that derived from the A14 curve. Figure 1c shows the differences between the best-fit model color-excesses for A14 and that of the FTZ model for A14, the CSMD model for F14, as well as the best-fit model for F14. They are generally within the observational uncertainties. However, as shown in Figure 2, the model extinction at $\lambda < 0.3 \mu\text{m}$ differs considerably from the CCM parameterization. The latter is known to be invalid for extragalactic sightlines.

In Figure 4 we show the dust size distributions derived from the models with $[\text{C}/\text{H}]_{\text{dust}} = 83.2$, 41.6 and 0 ppm. Compared with that of the MW average of $R_V = 3.1$ [Mathis et al. 1977 (hereafter MRN); Weingartner & Draine 2001 (hereafter WD01)], the size distributions of the dust in the ISM toward SN 2014J are skewed toward substantially smaller grains. The MRN size distribution is a power-law $dn/da \propto a^{-3.5}$ in the size range of $50 \text{ \AA} < a < 0.25 \mu\text{m}$ for both dust components. The WD01 size distributions extend the lower cutoff size to $a_{\text{min}} = 3.5 \text{ \AA}$ with the smallest grains ($a \lesssim 50 \text{ \AA}$) constrained by the near- and mid-IR emission (see Li & Draine 2001). The dust model presented here for SN 2014J assumes $a_{\text{min}} = 50 \text{ \AA}$ since the UV extinction cannot constrain the exact size of nano-sized dust (see Li 2004).

5. DISCUSSION

5.1. The Extinction Curves

The host galaxy of SN 2014J, M82, is regarded as one of the archetypical starburst and superwind galaxies. Calzetti et al. (1994) derived the internal dust extinction in starbursts from their overall emission spectra. The inferred attenuation curve is much flatter than that derived for SN 2014J (see Figure 3). While the SN 2014J model extinction curves for $[\text{C}/\text{H}]_{\text{dust}} > 0$ exhibit an appreciable bump at 2175 \AA (e.g., $\Delta\tau_{2175} \approx 1.8$ for the $[\text{C}/\text{H}]_{\text{dust}} \approx 83.2 \text{ ppm}$ model), the starburst attenuation curve shows no evidence for the 2175 \AA bump. It is not clear to what extent the flatness of the apparent starburst attenuation curve may be due to the effects of radiative transfer in optically thick distributions of stars and dust.

Hutton et al. (2014) analyzed the UV images of M82 taken by the *UV/Optical Telescope (UVOT)* on board *Swift*. The color-color diagram obtained with the UVW2 (2033 \AA), UVM2 (2229 \AA), and UVW1 (2591 \AA) filters is especially sensitive to the presence of the 2175 \AA bump. They examined the color-color diagram and argued against a “bump-less” Calzetti-type law.

In the silicate-graphite model presented here, the 2175 \AA extinction bump is produced by small graphite dust. If we consider amorphous carbon (Rouleau & Martin 1991) instead of graphite, the

2175 Å bump will be absent. Excellent fits can also be obtained from a mixture of silicate and amorphous carbon (see Table 1). Unfortunately, neither the A14 color-excess data points nor the F14 extinction curve covered the 2175 Å bump. Due to the lack of spectral features (e.g., the 2175 Å bump), we are not able to constrain the exact composition and quantity of the carbon dust component (see Table 1).

The extinction laws derived for SN 2014J are even steeper than that of the SMC bar (see Figure 3); correspondingly, the dust sizes of SN 2014J are smaller than that of the SMC bar (see Figure 4). This may be related to the intense UV radiation and shocks associated with star formation in M82 that could destroy the dust and lead to a predominance of small grains.

In addition to the 2175 Å bump, the models presented here also predict two absorption features around 9.7 and 18 μm arising from amorphous silicate (see Figure 3). Depending on $[\text{C}/\text{H}]_{\text{dust}}$, the optical depth of the 9.7 μm feature ($\Delta\tau_{9.7}$) ranges from ~ 0.34 to ~ 0.86 . Beirão et al. (2008) reported the detection of the 9.7 μm feature in the *Spitzer*/IRS spectra of the central region of M82, with an optical depth of $\Delta\tau_{9.7} \approx 0.3$ –3.1. Telesco et al. (2015) obtained the ~ 8 –13 μm mid-IR spectra of SN 2014J at 57 to 137 days after explosion and did not detect the 9.7 μm feature.

5.2. R_V

It is often suggested that the extinction laws toward SNe Ia are “non-standard” or “unusual” in the sense that unlike the MW mean value of $R_V \approx 3.1$, SNe Ia often have a much smaller R_V (see Figure 3 of Howell 2011), indicating steep UV extinction.

There are several examples of highly reddened SNe Ia for which R_V can be measured directly. They all have $R_V \lesssim 2$ (e.g., Krisciunas et al. 2006; Elias-Rosa et al. 2006, 2008; Nobili & Goobar 2008; Wang et al. 2008; Folatelli et al. 2010). However, many low reddened [$E(B - V) < 0.3 \text{ mag}$] ones have R_V values close to that of the MW (Mandel et al. 2011; Phillips 2012). On the other hand, statistical studies of large samples of SNe Ia have found $R_V < 2$ (e.g., Nobili et al. 2005; Guy et al. 2005; Hicken et al. 2009; Folatelli et al. 2010; Burns et al. 2011).⁶ Betoule et al. (2014) analyzed 740 low- and high- z SNe Ia and yields $R_V \sim 2$.

Many lines of evidence show that the reddening law to SN 2014J has a low value of $R_V \approx 1.4$ (see §4). Patat et al. (2015) and Kawabata et al. (2014) presented spectropolarimetric and optical/near-IR multi-band polarimetric observations of SN 2014J and both indicated a low value of $R_V < 2$. However, relatively larger R_V values have also been suggested for SN 2014J. Using the equivalent widths of 10 diffuse interstellar bands, Welty et al. (2014) yielded $E(B - V) \sim 0.71 \pm 0.11 \text{ mag}$

and $R_V \approx 2.7$ for SN 2014J.

The extinction curves A_λ/A_V and R_V values derived here for SN 2014J are based on detailed dust modeling of the observed color excesses. They are generally consistent with previous studies of $R_V < 2$ for SN 2014J. However, we caution the use of R_V to derive an extinction law for SN 2014J (or any extragalactic sightlines) since, as demonstrated in Figure 3, the model extinction curves differ substantially from that calculated from the CCM formula.

5.3. *Interstellar or Circumstellar?*

It has been suggested that multiple scattering by circumstellar dust surrounding their progenitors could explain the non-standard reddening observed in the lines of sight to SNe Ia (Wang 2005; Goobar 2008; Amanullah & Goobar 2011). However, F14 argued that the wide range of observed properties for SN 2014J may be caused by a combination of interstellar reddening and scattering off circumstellar material. Johansson et al. (2014) analyzed the 3.6 and 4.5 μm *Spitzer*/IRAC data of SN 2014J and detected no significant IR excess. They hence placed an upper limit of $M_{\text{dust}} \lesssim 10^{-5} M_\odot$ on the pre-existing dust in the circumstellar environment of SN 2014J. This is insufficient to account for the observed non-standard reddening. Moreover, Brown et al. (2015) analyzed the light curves and color evolution obtained with *Swift*/UVOT. They argued that these observations are inconsistent with a contribution scattered into the line of sight by circumstellar dust.

6. CONCLUSIONS

The extinction toward SN 2014J in M82 is derived as a function of wavelength from fitting the observed color excesses with a mixture of silicate and graphite or amorphous carbon dust. Insensitive to the exact carbon dust composition and quantity, the model derives $A_V \approx 1.9 \text{ mag}$, $E(B - V) \approx 1.1 \text{ mag}$, and $R_V \approx 1.7$, generally consistent with those reported in the literature.

We thank the anonymous referee and S. Wang for helpful suggestions. This work is supported by NSFC 11173007, 11373015, 11178003, and 11325313, 973 Program 2014CB845702 and 2013CB834903, NSF AST-1109039, NNX13AE63G, and the Fundamental Research Funds for the Central Universities.

⁶ However, it has also been suggested that the low values of R_V derived from large samples may partly result from the poor assumptions about the intrinsic color distribution of SNe Ia (e.g., see Foley et al. 2011; Mandel et al. 2011).

TABLE 2
MODELED EXTINCTION TOWARDS SN 2014J^a

Band	λ (μm)	[C/H] _{dust} = 41.6ppm		[C/H] _{dust} = 81.3ppm	
		A_λ (mag)	C_{ext} (cm^2/H)	A_λ (mag)	C_{ext} (cm^2/H)
Ly edge	0.091	39.87	2.06×10^{-21}	29.32	2.22×10^{-21}
Ly α	0.122	29.40	1.52×10^{-21}	22.85	1.73×10^{-21}
UVW2/UVOT	0.203	13.87	7.16×10^{-22}	13.09	9.92×10^{-22}
UVM2/UVOT	0.223	12.53	6.47×10^{-22}	12.44	9.43×10^{-22}
UVW1/UVOT	0.259	8.64	4.46×10^{-22}	8.63	6.54×10^{-22}
F225W/HST	0.287	6.98	3.60×10^{-22}	6.96	5.28×10^{-22}
F275W/HST	0.290	6.84	3.53×10^{-22}	6.82	5.17×10^{-22}
F218W/HST	0.311	5.97	3.08×10^{-22}	5.96	4.52×10^{-22}
F336W/HST	0.340	5.03	2.59×10^{-22}	5.02	3.81×10^{-22}
<i>u</i> /SDSS	0.355	4.63	2.39×10^{-22}	4.62	3.50×10^{-22}
U	0.365	4.39	2.27×10^{-22}	4.39	3.33×10^{-22}
F438W/HST	0.433	3.15	1.63×10^{-22}	3.16	2.40×10^{-22}
B	0.440	3.06	1.58×10^{-22}	3.06	2.32×10^{-22}
F467M/HST	0.468	2.70	1.39×10^{-22}	2.71	2.05×10^{-22}
<i>g</i> /SDSS	0.469	2.69	1.39×10^{-22}	2.70	2.05×10^{-22}
V	0.550	1.94	1.00×10^{-22}	1.94	1.47×10^{-22}
F555W/HST	0.550	1.94	1.00×10^{-22}	1.94	1.47×10^{-22}
<i>r</i> /SDSS	0.617	1.54	7.93×10^{-23}	1.53	1.16×10^{-22}
F631N/HST	0.630	1.48	7.62×10^{-23}	1.47	1.12×10^{-22}
R	0.700	1.19	6.13×10^{-23}	1.18	8.98×10^{-23}
<i>i</i> /SDSS	0.748	1.04	5.35×10^{-23}	1.03	7.82×10^{-23}
F814W/HST	0.792	0.92	4.75×10^{-23}	0.92	6.95×10^{-23}
F845M/HST	0.863	0.77	3.99×10^{-23}	0.77	5.83×10^{-23}
<i>z</i> /SDSS	0.893	0.72	3.72×10^{-23}	0.72	5.44×10^{-23}
I	0.900	0.71	3.66×10^{-23}	0.71	5.35×10^{-23}
J/2MASS	1.235	0.38	1.94×10^{-23}	0.37	2.82×10^{-23}
H/2MASS	1.662	0.22	1.14×10^{-23}	0.22	1.64×10^{-23}
Ks/2MASS	2.159	0.15	7.53×10^{-24}	0.14	1.07×10^{-23}
W1/WISE	3.353	0.08	4.32×10^{-24}	0.08	5.83×10^{-24}
L	3.450	0.08	4.18×10^{-24}	0.07	5.63×10^{-24}
[3.6]/IRAC	3.545	0.08	4.06×10^{-24}	0.07	5.45×10^{-24}
[4.5]/IRAC	4.442	0.06	3.18×10^{-24}	0.05	4.13×10^{-24}
W2/WISE	4.603	0.06	3.07×10^{-24}	0.05	3.97×10^{-24}
M	4.800	0.06	2.96×10^{-24}	0.05	3.81×10^{-24}
[5.8]/IRAC	5.675	0.05	2.78×10^{-24}	0.05	3.42×10^{-24}
[8.0]/IRAC	7.760	0.10	5.20×10^{-24}	0.07	5.60×10^{-24}
N	10.600	0.40	2.06×10^{-23}	0.28	2.08×10^{-23}
W3/WISE	11.561	0.27	1.40×10^{-23}	0.19	1.42×10^{-23}
Q	21.000	0.16	8.10×10^{-24}	0.11	8.34×10^{-24}
W4/WISE	22.088	0.14	7.21×10^{-24}	0.10	7.47×10^{-24}

^aThe extinction results with [C/H]_{dust} = 41.6ppm are recommended. Because of the space limitation of ApJL, this table is not shown in the published version of this Letter.

REFERENCES

- Amanullah, R., & Goobar, A. 2011, *ApJ*, 735, 20
- Amanullah, R., Goobar, A., Johansson, J., et al. 2014, *ApJ*, 788, L21
- Ashall, C., Mazzali, P., Bersier, D., Hachinger, S., Phillips, M., Percival, S., James, P., & Maguire, K. 2014, *MNRAS*, 445, 4424
- Beirão, P., Brandl, B. R., Appleton, P. N., et al. 2008, *ApJ*, 676, 304
- Betoule, M., Kessler, R., Guy, J., et al. 2014, *A&A*, 568, A22
- Brown, P. J., Smitka, M. T., Wang, L., et al. 2015, *ApJ*, 805, 74
- Burns, C. R., Stritzinger, M., Phillips, M. M., et al. 2011, *AJ*, 141, 19
- Calzetti, D., Kinney, A. L., & Storchi-Bergmann, T. 1994, *ApJ*, 429, 582
- Cardelli, J. A., Clayton, G. C., & Mathis, J. S. 1989, *ApJ*, 345, 245
- Cardelli, J. A., Meyer, D. M., Jura, M., & Savage, B. D. 1996, *ApJ*, 467, 334
- Dalcanton, J. J., Williams, B. F., Seth, A. C., et al. 2009, *ApJS*, 183, 67
- Draine, B. T., & Lee, H. M. 1984, *ApJ*, 285, 89
- Elias-Rosa, N., Benetti, S., Cappellaro, E., et al. 2006, *MNRAS*, 369, 1880
- Elias-Rosa, N., Benetti, S., Turatto, M., et al. 2008, *MNRAS*, 384, 107
- Fitzpatrick, E. L. 1999, *PASP*, 111, 63
- Folatelli, G., Phillips, M. M., Burns, C. R., et al. 2010, *AJ*, 139, 120
- Foley, R. J., Sanders, N. E., & Kirshner, R. P. 2011, *ApJ*, 742, 89
- Foley, R. J., Fox, O. D., McCully, C., et al. 2014, *MNRAS*, 443, 2887
- Goobar, A. 2008, *ApJ*, 686, L103
- Goobar, A., Johansson, J., Amanullah, R., et al. 2014, *ApJ*, 784, L12
- Gordon, K. D., Clayton, G. C., Misselt, K. A., Landolt, A. U., & Wolff, M. J. 2003, *ApJ*, 594, 279
- Grevesse, N., & Sauval, A. J. 1998, *Space Sci. Rev.*, 85, 161
- Guy, J., Astier, P., Nobili, S., Regnault, N., & Pain, R. 2005, *A&A*, 443, 781
- Hicken, M., Challis, P., Jha, S., et al. 2009, *ApJ*, 700, 331
- Howell, D. A. 2011, *Nature Communications*, 2, 350
- Hutton, S., Ferreras, I., Wu, K., Kuin, P., Breeveld, A., Yershov, V., Cropper, M., & Page, M. 2014, *MNRAS*, 440, 150
- Johansson, J., Goobar, A., Kasliwal, M. M., et al. 2014, arXiv:1411.3332
- Kawabata, K. S., Akitaya, H., Yamanaka, M., et al. 2014, *ApJ*, 795, L4
- Krisciunas, K., Prieto, J. L., Garnavich, P. M., Riley, J.-L. G., Rest, A., Stubbs, C., & McMillan, R. 2006, *AJ*, 131, 1639
- Li, A. 2004, in *Astrophysics of Dust*, Witt, A.N., Clayton, G.C., & Draine, B.T. (eds.), ASP Conf. Ser., 309, 417
- Li, A., & Draine, B. T. 2001, *ApJ*, 554, 778
- Li, A., Misselt, K. A., & Wang, Y. J. 2006, *ApJ*, 640, L151
- Mandel, K. S., Narayan, G., & Kirshner, R. P. 2011, *ApJ*, 731, 120
- Marion, G. H., Sand, D. J., Hsiao, E. Y., et al. 2015, *ApJ*, 798, 39
- Mathis, J. S., Rimpl, W., & Nordsieck, K. H. 1977, *ApJ*, 217, 425 (MRN)
- Nobili, S., & Goobar, A. 2008, *A&A*, 487, 19
- Nobili, S., Amanullah, R., Garavini, G., et al. 2005, *A&A*, 437, 789
- Origlia, L., Ranalli, P., Comastri, A., & Maiolino, R. 2004, *ApJ*, 606, 862
- Patat, F., Taubenberger, S., Cox, N. L. J., et al. 2015, *A&A*, 577, A53
- Perlmutter, S., Aldering, G., Goldhaber, G., et al. 1999, *ApJ*, 517, 565
- Phillips, M. M. 2012, *PASA*, 29, 434
- Riess, A. G., Filippenko, A. V., Challis, P., et al. 1998, *AJ*, 116, 1009
- Rouleau, F., & Martin, P. G. 1991, *ApJ*, 377, 526
- Telesco, C. M., Höflich, P., Li, D., et al. 2015, *ApJ*, 798, 93
- Wang, L. 2005, *ApJ*, 635, L33
- Wang, X., Li, W., Filippenko, A. V., et al. 2008, *ApJ*, 675, 626
- Weingartner, J. C., & Draine, B. T. 2001, *ApJ*, 548, 296 (WD01)
- Welty, D. E., Ritchey, A. M., Dahlstrom, J. A., & York, D. G. 2014, *ApJ*, 792, 106